PHILOSOPHICAL TRANSACTIONS OF THE ROYAL SOCIETY A MATHEMATICAL, PHYSICAL & ENGINEERING SCIENCES

Modelling of spherical gas bubble oscillations and sonoluminescence

A. Prosperetti and Y. Hao

Phil. Trans. R. Soc. Lond. A 1999 **357**, 203-223
doi: 10.1098/rsta.1999.0324

THE ROYAL SOCIETY

Modelling of spherical gas bubble oscillations and sonoluminescence

By A. Prosperetti and Y. Hao

Department of Mechanical Engineering, The Johns Hopkins University, Baltimore, MD 21218, USA

The discovery of single-bubble sonoluminescence has led to a renewed interest in the forced radial oscillations of gas bubbles. Many of the more recent studies devoted to this topic have used several simplifications in the modelling, and in particular in accounting for liquid compressibility and thermal processes in the bubble. In this paper the significance of these simplifications is explored by contrasting the results of Lohse and co-workers with those of a more detailed model. It is found that, even though there may be little apparent difference between the radius-versus-time behaviour of the bubble as predicted by the two models, quantities such as the spherical stability boundary and the threshold for rectified diffusion are affected in a quantitatively significant way. These effects are a manifestation of the subtle dependence upon dissipative processes of the phase of radial motion with respect to the driving sound field. The parameter space region, where according to the theory of Lohse and co-workers, sonoluminescence should be observable, is recalculated with the new model and is found to be enlarged with respect to the earlier estimate. The dependence of this parameter region on sound frequency is also illustrated.

Keywords: bubble dynamics; sonoluminescence; acoustic caviation; rectified diffusion

1. Introduction

The intriguing phenomenon of single-bubble sonoluminescence (Gaitan & Crum 1990; Gaitan *et al*. 1992; Barber *et al*. 1997) has prompted a renewed interest in the behaviour of oscillating gas bubbles. With few exceptions (see, for example, Lepoint *et al*. 1997; Longuet-Higgins 1996, 1997, 1998; Prosperetti 1997), the theoretical studies devoted to the phenomenon have been based on the assumption of a spherical bubble (see, for example, Kamath *et al*. 1993; Kondić *et al*. 1995, 1998; Moss *et al*. 1994, 1997; Chu 1996; Yuan *et al*. 1998). Among the models proposed, that of Lohse and co-workers (Brenner *et al*. 1995, 1996; Lohse *et al*. 1997; Lohse & Hilgenfeldt 1997; Hilgenfeldt *et al*. 1996, 1998, 1999) stands out as it furnishes a comprehensive picture of the phenomenon, free of adjustable parameters and capable of explaining many of the experimental observations.

From the point of view of bubble dynamics, this model is of great interest as it brings together a great many facets of the subject and can therefore serve as a unified setting in which to study and demonstrate many of the physical aspects of oscillating gas bubbles, such as mass diffusion, stability, and others. The specific purpose of the present paper is to examine how the original results of Lohse and co-workers are modified by the use of more realistic mathematical models for the various physical

processes that it incorporates. Since, however, these processes are encountered widely in fields such as acoustic cavitation, sonochemistry, and others, in spite of its focus on sonoluminescence, the present paper can be expected to be relevant for other phenomena as well. For additional background information on the forced oscillations of gas bubbles, several reviews are available (see, for example, Plesset & Prosperetti 1977; Apfel 1981; Prosperetti 1984*a*, *b*; Leighton 1994).

According to the model of Lohse and co-workers the region of parameter space in which sonoluminescence can be observed is bounded by several curves that describe thresholds for rectified diffusion, stability of the spherical shape, temperature conditions in the bubble, etc. After a presentation of the mathematical model for radial oscillations in §§ 2–4, in the sections that follow we present results for these quantities comparing them with those of Lohse *et al*. According to the interpretation of single-bubble sonoluminescence that they propose, after an initial transient, the bubble will remain filled only with an inert gas which, in experiments, would be most commonly argon. Hence, in all our simulations (except one, where we compare with data obtained with air bubbles), we shall assume the gas to be monatomic with a ratio of specific heats $\gamma = \frac{5}{3}$ and with the physical properties of argon.

2. The radial equation of motion

A useful form of the equation describing the radial dynamics of the bubble accounting to first order for liquid compressibility was given by Keller and co-workers (Keller & Kolodner 1956; Keller & Miksis 1980):

$$\left(1-\frac{\dot R}{c_{\rm L}}\right)R\ddot R+\frac{3}{2}\left(1-\frac{1}{3}\frac{\dot R}{c_{\rm L}}\right)\dot R^2 = \frac{1}{\rho_{\rm L}}\left(1+\frac{\dot R}{c_{\rm L}}+\frac{R}{c_{\rm L}}\frac{\mathrm{d}}{\mathrm{d}t}\right)[p_{\rm B}-P_\infty-P_{\rm S}(t)]+O(c_{\rm L}^{-2}). \tag{2.1}$$

In this equation dots denote time derivatives, $c_{\rm L}$ is the speed of sound in the liquid, P_∞ is the static ambient pressure, $P_{\rm S}(t)$ is the imposed acoustic field pressure evaluated at the location of the bubble and $p_{\rm B}$ is the pressure on the liquid side of the interface. This quantity is related to the bubble internal pressure p by the balance of normal stresses across the interface, namely

$$p = p_{\rm B}+\frac{2\sigma}{R}+4\mu\frac{\dot R}{R}, \tag{2.2}$$

in which σ is the surface tension coefficient and μ the liquid viscosity. In this study we take the sound field to be sinusoidal:

$$P_{\rm S}(t) = P_{\rm A}\cos\omega t, \tag{2.3}$$

with $P_{\rm A}$ the acoustic amplitude and ω the driving angular frequency.

The issue of the compressibility corrections to the Rayleigh–Plesset equation was examined in detail in Prosperetti & Lezzi (1986) and Lezzi & Prosperetti (1987). There it was shown, by comparison with a numerical calculation fully accounting for the liquid compressibility, that a preferable form made use of the equation of state

of the liquid to write the equation in terms of the enthalpy†:

$$\left(1-\frac{\dot{R}}{c_{\mathrm{L}}}\right)R\ddot{R}+\frac{3}{2}\left(1-\frac{1}{3}\frac{\dot{R}}{c_{\mathrm{L}}}\right)\dot{R}^2 = \left(1+\frac{\dot{R}}{c_{\mathrm{L}}}+\frac{R}{c_{\mathrm{L}}}\frac{\mathrm{d}}{\mathrm{d}t}\right)\left[h_{\mathrm{B}}-\frac{1}{\rho_{\mathrm{L}}}P_{\mathrm{S}}\left(t+\frac{R}{c_{\mathrm{L}}}\right)\right]+O(c_{\mathrm{L}}^{-2}), \tag{2.4}$$

where

$$h_{\mathrm{B}}=\int_{P_\infty}^{p_{\mathrm{B}}}\frac{\mathrm{d}p}{\rho} \tag{2.5}$$

is the liquid enthalpy evaluated in correspondence of the pressure p_{B} at the bubble surface. A widely used equation of state for liquids is the Tait form:

$$\frac{p+B}{P_\infty+B}=\left(\frac{\rho}{\rho_{\mathrm{L}}}\right)^n, \tag{2.6}$$

where $\rho_{\mathrm{L}}=\rho(P_\infty)$ and n, B are constants having, for water, the values $n=7.15$, $B=3049.13$ atm. With this equation of state we find

$$h_{\mathrm{B}}=\frac{1}{n-1}(c_{\mathrm{B}}^2-c_{\mathrm{L}}^2),\quad c_{\mathrm{L}}^2=n\frac{P_\infty+B}{\rho_{\mathrm{L}}}, \tag{2.7}$$

with c_{B}^2 given by a similar formula with p_{B} in place of P_∞.

Superficially, equations (2.1) and (2.4) suffer from the unphysical behaviour that acceleration and pressure difference have opposite sign when the bubble-wall Mach number $Ma=|\dot{R}|/c_{\mathrm{L}}$ exceeds unity. In principle, the situation is quite clear: both equations were derived under the assumption of small Ma, and therefore any wrong behaviour at $Ma\sim 1$ is not unexpected, but simply the consequence of pushing an approximation beyond its domain of validity. In spite of this limitation, essentially all the recent work on the application of spherical bubble dynamics to sonoluminescence has been based on some form of these equations‡. The argument is that one encounters large velocities only over a minute fraction of the oscillation cycle and therefore, provided some reasonable means of 'interpolating' the radial motion across these short time intervals is used, the error should not be too large. For this reason, to ameliorate the unphysical behaviour previously mentioned, many workers have used the original form of Herring (1941; see also Cole 1948, ch. 8; Vokurka 1986; Ilinskii & Zabolotskaya 1992), which replaces the offending terms $(1\pm\dot{R}/c_{\mathrm{L}})$, $(1-\dot{R}/3c_{\mathrm{L}})$ by unity (Löfstedt *et al.* 1993; Hilgenfeldt *et al.* 1996; Lohse & Hilgenfeldt 1997; Matula *et al.* 1997). Thus, for example, the equation used in the work of Lohse and

† By the manner of the derivation of this equation, c_{L} and ρ_{L} are to be evaluated at equilibrium and treated as constants. According to an alternative form of the equation, obtained with the aid of the so-called Kirkwood–Bethe approximation, c_{L} is evaluated at the bubble surface using the local pressure conditions. From a mathematical standpoint, the Kirkwood–Bethe approximation is not any better than the small-Mach-number theory of the cited references, and therefore there is no *a priori* reason to prefer a variable c_{L} to a constant c_{L}. The matter has not been explored on the basis of actual numerical accuracy. Here we treat c_{L} and ρ_{L} as constants, except in carrying out the integration in (2.5).

‡ An equation valid to the next order in Ma was given in Lezzi & Prosperetti (1987), but it fails to shed much light on how to improve on (2.4) due to a severe lack of uniqueness.

co-workers is†:

$$R\ddot{R} + \tfrac{3}{2}\dot{R}^2 = \frac{1}{\rho_{\mathrm{L}}}\left(1 + \frac{R}{c_{\mathrm{L}}}\frac{\mathrm{d}}{\mathrm{d}t}\right)(p - P_\infty - P_{\mathrm{S}}(t)) - \frac{4\mu\dot{R}}{\rho_{\mathrm{L}}R} - \frac{2\sigma}{\rho_{\mathrm{L}}R}. \tag{2.8}$$

Here we use what we believe to be a slightly better approximation, which avoids the sign change of $(1 \pm \dot{R}/c_{\mathrm{L}})$ when $|\dot{R}/c_{\mathrm{L}}|$ crosses unity while still retaining the *correct* information contained in these terms over the large fraction of the cycle where the Mach number is small. We simply note that

$$1 \pm \frac{\dot{R}}{c_{\mathrm{L}}} = \frac{1}{1 \mp \dot{R}/c_{\mathrm{L}}} + O(Ma)^2, \tag{2.9}$$

and therefore, when $\dot{R}/c_{\mathrm{L}} > 0$, we write equation (2.4) as

$$\frac{1}{1 + \dot{R}/c_{\mathrm{L}}}R\ddot{R} + \frac{3}{2}\left(1 - \frac{1}{3}\frac{\dot{R}}{c_{\mathrm{L}}}\right)\dot{R}^2 = \left(1 + \frac{\dot{R}}{c_{\mathrm{L}}} + \frac{R}{c_{\mathrm{L}}}\frac{\mathrm{d}}{\mathrm{d}t}\right)\left[h_{\mathrm{B}} - \frac{1}{\rho_{\mathrm{L}}}P_{\mathrm{S}}\left(t + \frac{R}{c_{\mathrm{L}}}\right)\right], \tag{2.10}$$

while when $\dot{R}/c_{\mathrm{L}} < 0$, we write

$$\left(1 - \frac{\dot{R}}{c_{\mathrm{L}}}\right)R\ddot{R} + \frac{3}{2}\left(1 - \frac{1}{3}\frac{\dot{R}}{c_{\mathrm{L}}}\right)\dot{R}^2 = \left(\frac{1}{1 - \dot{R}/c_{\mathrm{L}}} + \frac{R}{c_{\mathrm{L}}}\frac{\mathrm{d}}{\mathrm{d}t}\right)\left[h_{\mathrm{B}} - \frac{1}{\rho_{\mathrm{L}}}P_{\mathrm{S}}\left(t + \frac{R}{c_{\mathrm{L}}}\right)\right]. \tag{2.11}$$

The switching between the two forms of the equation is done when $\dot{R}$ goes through zero, which preserves a desirable degree of continuity. One could also subject to the same treatment the coefficient of $\dot{R}^2$, but, since in our simulations we have never found a Mach number larger than about 2, this is unnecessary.

3. The bubble interior

The mathematical model for the bubble interior is described in detail in Prosperetti *et al*. (1988), Kamath & Prosperetti (1989) and Prosperetti (1991). The model accounts for the compressibility of the gas and heat transport by convection and by conduction inside the bubble. The main assumptions, discussed below, are those of perfect-gas behaviour and of spatial uniformity of the gas pressure.

The internal pressure p is found by integrating

$$\dot{p} = \frac{3}{R}\left[(\gamma - 1)k\left.\frac{\partial T}{\partial r}\right|_R - \gamma p\dot{R}\right], \tag{3.1}$$

where γ is the ratio of the specific heats of the gas and k is the gas thermal conductivity. The gas temperature field $T(r, t)$ is obtained from

$$\frac{\gamma}{\gamma - 1}\frac{p}{T}\left(\frac{\partial T}{\partial t} + v\frac{\partial T}{\partial r}\right) = \dot{p} + \frac{1}{r^2}\frac{\partial}{\partial r}\left(kr^2\frac{\partial T}{\partial r}\right), \tag{3.2}$$

† It will be noted that this equation differs from (2.1) in the minor aspect that the terms arising from the time differentiation of the surface tension and viscous contributions when (2.2) is substituted into (2.1) are not retained.

with

$$v = \frac{1}{\gamma p}\left[(\gamma - 1)k\frac{\partial T}{\partial r} - \tfrac{1}{3}r\dot{p}\right]. \tag{3.3}$$

These results are exact under the hypotheses mentioned before.

In order to avoid dealing with the energy equation in the liquid, the gas energy equation (3.2) is solved assuming that the liquid temperature at the surface of the bubble remains undisturbed. In Kamath *et al.* (1993) it was shown that surface temperature changes had only a minor effect. Here the acoustic pressures considered are larger than in that study and the gas temperatures correspondingly higher. The status of the approximation is thus not as clear. If liquid temperatures at the bubble wall rise considerably, phase-change effects should be modelled. This problem has received insufficient attention.

In deriving (3.2) the gas specific heat is assumed to be constant. Since the specific heat of gases is an increasing function of temperature, this approximation will tend to overpredict the gas temperature somewhat. For the temperature dependence of the gas thermal conductivity k, we use the kinetic-theory result (Amdur & Mason 1958)

$$k = 0.265\,26 \times 10^{-3} T^{0.74}, \tag{3.4}$$

where k is in W m^{-1} K and T in K.

As for the assumption of spatially uniform pressure, it of course rules out the presence of shock waves. The recent results of Vuong *et al.* (1999) and Yuan *et al.* (1998) cast some doubts on the formation of shocks. Furthermore, already in the first study devoted to the matter, Trilling (1952) found that shock waves (if any) do not affect the bubble-wall motion to any great degree, a conclusion that has been confirmed more recently by Kondić *et al.* (1995). Moss *et al.* (1997) find that the instant at which the radial motion reverses coincides with the arrival of the shock reflected from the bubble centre to its surface. However, they do not attribute a particular importance to this fact as the increase in gas pressure would in itself be sufficient to stop the collapse of the bubble. Even if shocks are important for the mechanism of sonoluminescent emission (a fact on which, as noted before, recent research casts some doubt), they are not necessarily so for the other aspects of bubble dynamics (stability, rectified diffusion, etc.) that are thought to establish the conditions for the phenomenon to occur. Since our interest in the next sections is in these latter aspects, we feel justified in adopting the assumption of a spatially uniform internal pressure.

Lohse *et al.* use a simplified model for the calculation of the bubble internal pressure and temperature. For the former they adopt the relation

$$p = \left(P_\infty + \frac{2\sigma}{R_0}\right)\left(\frac{R_0^3 - h^3}{R^3(t) - h^3}\right)^K, \tag{3.5}$$

where $h = R_0/8.86$ is the hard-core van der Waals radius for argon and the polytropic index K is taken to be unity. They stress that this is 'not an equation of state but rather a process equation'. The justification is that, due to the smallness of the bubble, over most of the cycle the gas in it is essentially isothermal, a conclusion that is in agreement with the behaviour shown in figures 4 and 5. The brief instants when conditions are different, they argue, are not going to have a significant impact

on the bubble dynamics. Evidently, equation (3.5) is not adequate to estimate the bubble-centre temperature T_c. For this purpose they use

$$\frac{T_c}{T_\infty} = \left(\frac{R_0^3 - h^3}{R^3(t) - h^3} \right)^{\kappa - 1}, \tag{3.6}$$

where the index κ is obtained from the linear-theory results of Prosperetti (1977*a*) and Plesset & Prosperetti (1977) by substituting $\dot{R}/R$ in place of ω^{-1} in the expression of the Péclet number.

For the numerical solution of the previous model, the gas energy equation is transformed into a set of ordinary differential equations by the Chebyshev spectral collocation method described in Kamath & Prosperetti (1989), after which the final ODE system is solved with the help of the subroutine LSODE. We used between 20 and 40 terms in the expansion depending on the acoustic pressure amplitude P_A. For the highest pressure amplitude, $P_A = 1.5$ bar, we used an even greater number of terms, finding essentially identical results. It was found that, if the number of expansion terms was insufficient, the solution settled down to a mildly chaotic regime rather than a periodic regime. A critical factor in the calculation was the use of a sufficiently large number of outputs per cycle to capture the extremely short duration of the temperature and velocity peaks.

4. Radial motion

Before proceeding to compare various quantities dependent on the radial motion, we examine here how the radial motion itself depends on the different assumptions discussed in the previous two sections. We choose a typical case studied by Hilgenfeldt *et al.* (1996), namely $R_0 = 4\,\mu$m, $P_A = 1.4$ bar, for which the driving is close to the upper limit of the range of present interest. The other conditions are $P_\infty = 1$ atm, $\rho_L = 1000\,\mathrm{kg\,m^{-3}}$, $\mu = 0.001\,\mathrm{kg\,m^{-1}\,s^{-1}}$, $\sigma = 0.07\,\mathrm{kg\,s^{-2}}$, $T_\infty = 20\,^\circ$C, $\omega/2\pi = 26.5$ kHz and $c_L = 1481\,\mathrm{m\,s^{-1}}$. These same parameter values are also used in the following. In all our examples we present results corresponding to steady-state motion.

We first consider the effect of the different versions of the radial equation of motion, using in all cases the model of § 3 for the calculation of the internal pressure and temperature. Figure 1 shows the radius versus time during steady oscillations. All the models give virtually identical results when plotted on this scale. To appreciate the differences we need to focus on the short time interval around the first collapse. Figure 2 is the radius versus time in this region. The solid line shows equations (2.10), (2.11), the short dashes show (2.1), the dash-dotted line is (2.4) and the long dashes show (2.8). Differences are small, but become noticeable if, in place of R, we consider the radial velocity (figure 3) and the centre temperature (figure 4). The form (2.8) is seen to predict a maximum value for $|\dot{R}|$ about a factor of two greater than the other models, thus implying that the neglected terms of order $\dot{R}/c_L$, while small, have an important effect when integrated over time. It is interesting to note from figure 4 that the corresponding centre temperature is, however, similar to that estimated on the basis of the other models. This result is due to the fact that the model (2.8) predicts a value of $\ddot{R}$ about 3.5 times greater than that given by (2.10), (2.11) with a consequent stronger reduction of the implosion velocity. Other than in the immediate

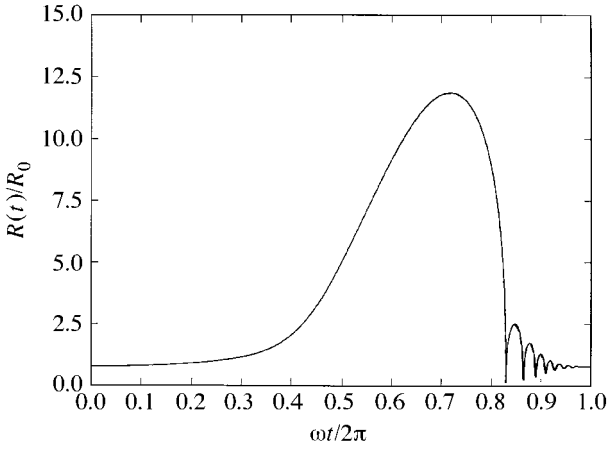

Figure 1. Radius versus time in the course of the steady oscillation of a 4 μm argon bubble under the action of a sound field with an acoustic amplitude of 1.4 bar and a frequency of 26.5 kHz. The solid line is the model (2.10), (2.11) and the (barely distinguishable) dashed line the model (2.8). The lines corresponding to the models of equations (2.1) and (2.4) cannot be distinguished on the scale of this figure. In all cases the internal pressure is calculated according to the complete model of § 3.

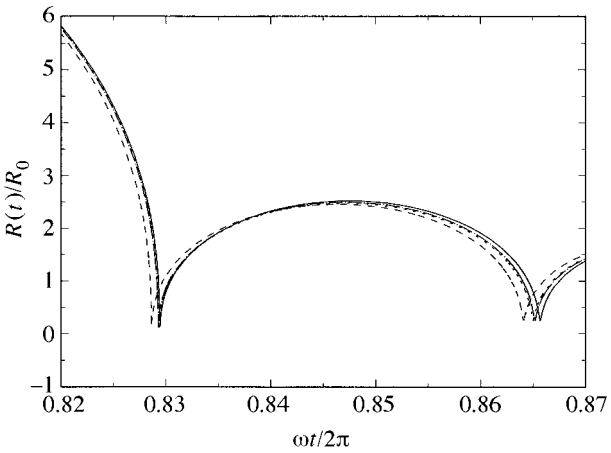

Figure 2. An enlargement of the previous figure in the neighbourhood of the first collapse: solid line, equations (2.10), (2.11); long dashes, equation (2.8); short dashes, equation (2.1); dash-and-dotted line, equation (2.4).

vicinity of the successive collapses, the centre temperature is close to the undisturbed value throughout the rest of the oscillations, as can be seen from figure 5.

In our earlier work (Kamath *et al.* 1993), we used a linear interpolation that well represented the gas thermal conductivity data up to a maximum temperature of about 3000 K, which is of the order of that encountered in that study, while here we use (3.4). Although the difference between the two temperature dependencies is considerable (for example, at a temperature of 50 000 K, (3.4) gives $k = 0.797$ W mK^{-1}, while the earlier form gives $k = 1.61$ W mK^{-1}), the final effect on the radial dynamics and the gas centre temperature is just a shift by about 0.4 ns of the instant

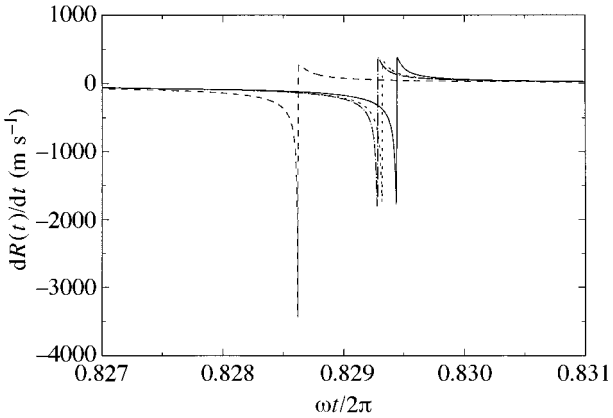

Figure 3. The radial velocity of the bubble of figures 1 and 2 in the neighbourhood of the first collapse illustrated in figure 2 as predicted by the models of § 2; in all cases the internal pressure is calculated according to the complete model of § 3: solid line, equations (2.10), (2.11); long dashes, equation (2.8); short dashes, equation (2.1); dash-and-dotted line, equation (2.4).

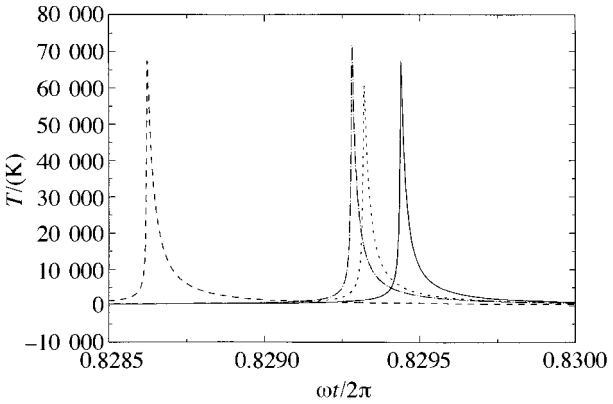

Figure 4. The centre temperature of the bubble of the previous figures in the neighbourhood of the first collapse illustrated in figures 2 and 3 as predicted by the models of § 2; in all cases the internal pressure is calculated according to the complete model of § 3: solid line, equations (2.10), (2.11); long dashes, equation (2.8); short dashes, equation (2.1); dash-and-dotted line, equation (2.4).

at which the maximum values of these quantities are attained. Figure 6 shows the temperature distribution in the bubble at the instants of maximum temperature as predicted with the expression (3.4) for k (solid line) and the linear relation used in our earlier work (dashed line).

Figures 7 and 8 compare the present model as given in equations (2.10)–(3.4), with the simplified model of Lohse and co-workers as given in equations (2.8), (3.5), (3.6), focusing only on the instants around the first collapse where the differences are greatest. Figure 7 shows the radial velocity and figure 8 the centre temperature, which are seen to be both greatly overpredicted by the simplified model†.

† We stress that the difference with the results presented in figures 3 and 4 is that there the complete

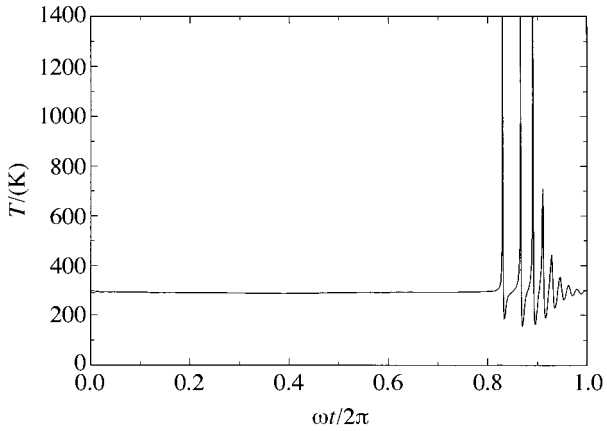

Figure 5. Centre temperature versus time during the steady oscillation of the bubble of figure 1 according to the complete model of §§ 2 and 3. In order to show details of the lower-temperature portion of the cycle, the vertical scale is not sufficiently extended to cover the maximum temperatures shown in the previous figure.

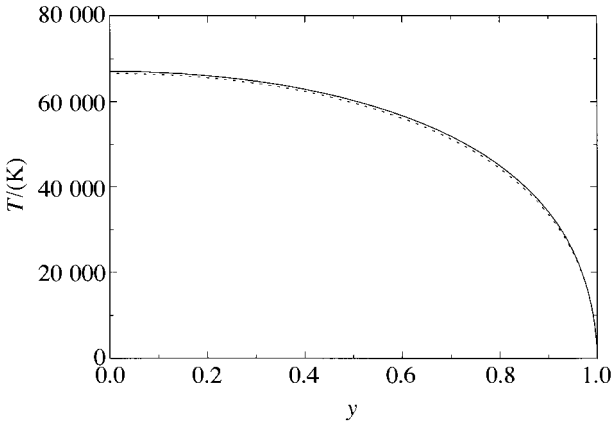

Figure 6. Gas temperature as a function of $y = r/R(t)$ at the instant of maximum temperature as calculated with the gas thermal conductivity k given by (3.4) (solid line), and with k given by a linear function of temperature (dashed line) for the conditions of figure 1.

Particularly during the last stages of the collapse, the behaviour of the gas in the bubble can deviate from that of a perfect gas, a matter that cannot be examined satisfactorily in the framework of our model. One can get a partial handle at least on the covolume effect by comparing the results obtained assuming p to be given by the adiabatic van der Waals relation, equation (3.5) with $K = \gamma$, with those obtained from the standard perfect-gas adiabatic relation. If the comparison is made at the same value of the acoustic amplitude P_A, it is found that the two models start deviating considerably for P_A greater than 1.15–1.2 bar. Since, however, the covolume effect depends on the minimum radius of the bubble, a more meaningful comparison is one made for minimum radii in the range predicted by the complete

model of § 3 was used for the bubble interior, while here the internal pressure and temperature are calculated from (3.5), (3.6).

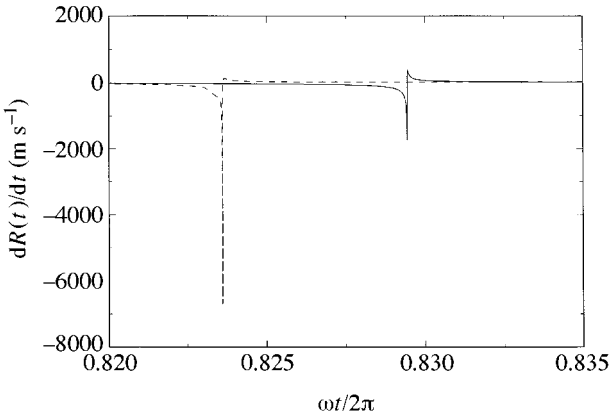

Figure 7. Comparison between the radial velocities given by the present model (solid line) and by that of Lohse and co-workers (dashed line) for the case of figure 1. The corresponding centre temperature is shown in the next figure. Unlike figure 3, where the only difference among models lies in the radial equation, here the results shown by the dashed line have been obtained using the relation (3.5) for the internal pressure.

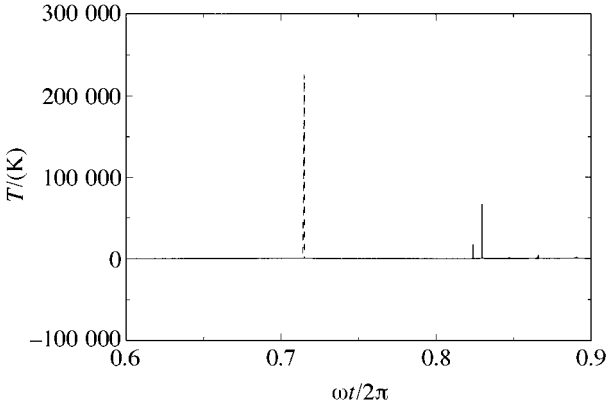

Figure 8. Comparison between the centre temperatures given by the present model (solid line) and by that of Lohse and co-workers (dashed line) for the case of figure 1. The corresponding radial velocities are shown in the previous figure.

model. For example, for $P_A = 1.4$ bar, which is close to the upper limit of interest here, the complete model gives a minimum radius of 0.48 μm. With the adiabatic perfect-gas model, the same minimum radius is found for $P_A = 1.105$ bar and, for this value of P_A, the difference with the hard-core van der Waals gas is negligible. The error induced by the neglect of the finite size of the molecules is therefore not expected to be of great significance.

5. Stability of the spherical shape

The equation governing the linear stability of the spherical shape of a bubble in a viscous liquid was derived in Prosperetti (1977*b*). This equation has an integro-differential structure and its numerical solution is a matter of some complexity. A

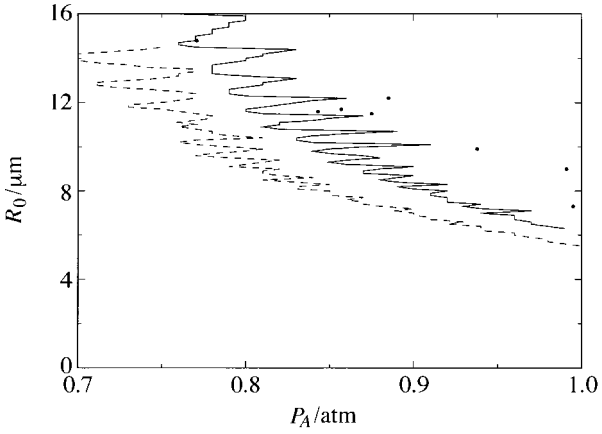

Figure 9. Comparison of the threshold for the parametric $n = 2$ instability as computed with the present model (solid line) and the model of Lohse and co-workers (dashed line) with the experimental data of Holt & Gaitan (1996) for air bubbles in water at a frequency of 20.6 kHz.

detailed description of the procedure and results will be published elsewhere (Hao & Prosperetti 1999). Suffice it to say here that those results show that, after an initial transient of a few cycles, the solution of the stability equation approaches very closely the solution of a boundary-layer approximation of the form (Prosperetti 1977*c*; Hilgenfeldt *et al*. 1996)

$$\ddot{a}_n + \left[3\frac{\dot{R}}{R} - 2(n-1)(n+1)(n+2)\frac{\mu}{\rho_{\mathrm{L}}R^2} + 2\frac{n(n+2)^2}{1+2\delta/R}\frac{\mu}{\rho_{\mathrm{L}}R^2}\right]\dot{a}_n + (n-1)\left[-\frac{\ddot{R}}{R} + (n+1)(n+2)\frac{\sigma}{\rho_{\mathrm{L}}R^3} + 2(n+2)\frac{\mu\dot{R}}{\rho_{\mathrm{L}}R^3}\left(n+1-\frac{n}{1+2\delta/R}\right)\right]a_n = 0, \tag{5.1}$$

where a_n is the amplitude of the nth surface mode and the boundary-layer thickness δ is approximated by

$$\delta = \min\left(\sqrt{\frac{\mu}{\rho_{\mathrm{L}}\omega}}, \frac{R}{2n}\right). \tag{5.2}$$

If we use in equation (5.1) the values of $R(t)$ and its derivatives provided by the mathematical model of the previous sections, we can calculate the parametric instability threshold of the different modes. A comparison with the recent data of Holt & Gaitan (1996) for air bubbles at a frequency of 20.6 kHz is shown in figure 9 for $n = 2$. Here the dots denote the data points corresponding to unstable modes identified as corresponding to $n = 2$. The solid line is the prediction of the present model and the dashed line that of Lohse and co-workers. It is clear that accounting for the thermal effects, as we do, improves agreement with the data even though the theoretical result is still somewhat below the data in the higher pressure amplitude range. It is shown in Hao & Prosperetti (1999) that this residual discrepancy is essentially removed if the exact integrodifferential formulation of viscous effects is adopted.

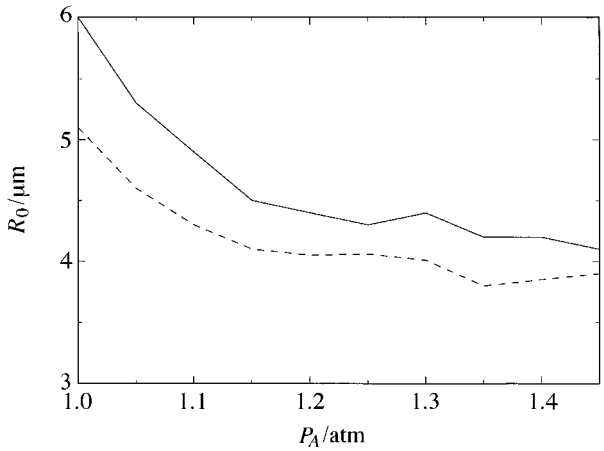

Figure 10. Comparison of the threshold for the parametric $n = 2$ instability as computed with the present model (solid line) and the model of Lohse and co-workers (dashed line) for argon bubbles at a frequency of 26.5 kHz.

Similar results for argon bubbles, in the higher pressure amplitude range of concern for sonoluminescence, are shown in figure 10, where again the stability threshold is increased by the effects included in the present model (solid line). In the parameter range of present concern, it is found that higher modes are more stable than $n = 2$, and therefore we do not show results for them.

A related instability mechanism, the so-called Rayleigh–Taylor instability, is also possible. Like its plane counterpart, it is due to the destabilizing effect of a positive value of $\ddot{R}$ in (5.1), and is therefore most marked near the point of minimum radius and the subsequent after-bounces. In contrast to the parametric instability, that develops over many cycles, the Rayleigh–Taylor instability is sudden in its manifestation and its effects may accumulate during the after-bounces following the time of minimum radius, but not from cycle to cycle†. This feature renders an evaluation of its impact on the phenomenon under consideration somewhat uncertain, as the maximum growth of the surface disturbance can only occur over a limited time. As a consequence, the maximum amplitude of the instability will depend on its initial value. Hilgenfeldt *et al.* (1996) subject the solution of (5.1) to a random perturbation of amplitude *ca.* 0.1 nm after each integration time step, and they declare the bubble unstable when the maximum value of $|a_2/R|$ over a cycle exceeds unity. Here we proceed differently by introducing a non-zero right-hand side in the stability equation (5.1). We have tried both a constant forcing and a superposition of the first hundred harmonics of the driving sound frequency with random amplitudes and phases. To present the results of these calculations for the model of Hilgenfeldt *et al.* (1996), we show in figure 11 the maximum value of a_2 over a cycle as a function of the bubble equilibrium radius for a few values of the forcing pressure amplitude P_{A}.

† Hilgenfeldt *et al.* (1996) distinguish between a Rayleigh–Taylor instability and an 'after-bounce instability', which can be considered as a parametric instability developing over the after-bounce cycles. This after-bounce instability will be all the more dangerous if the initial amplitude of the surface perturbation—itself a consequence of the Rayleigh–Taylor effect due to the first collapse—is large. For this reason we have not distinguished between the two instabilities, but we have grouped them together under the label 'Rayleigh–Taylor'.

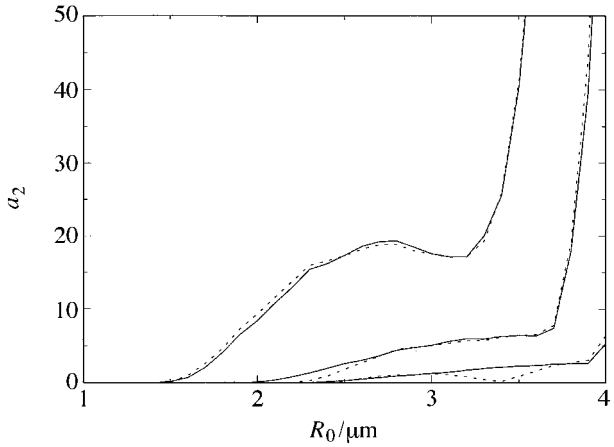

Figure 11. Maximum value reached by the amplitude a_2 of the $n = 2$ shape mode due to the Rayleigh–Taylor instability during one oscillation as predicted by equation (5.1) with a non-zero right-hand side. The solid lines are for a constant forcing, and the dashed lines for a random superposition of the first 100 harmonics of the driving frequency. The pressure amplitudes are, in descending order, 1.4, 1.3 and 1.25 bar. The instability thresholds reported by Hilgenfeldt *et al.* (1996) are $R_0 = 2.5$, 4 and 4.5 μm, respectively.

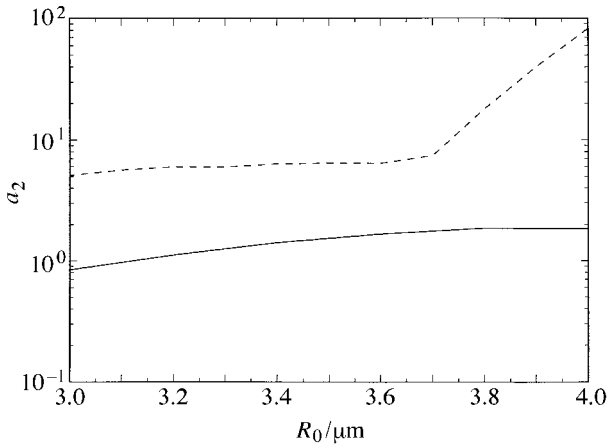

Figure 12. Maximum value reached by the amplitude a_2 of the $n = 2$ shape mode due to the Rayleigh–Taylor instability during one oscillation as predicted by equation (5.1) with a constant right-hand side for $P_A = 1.3$ bar. The results shown by the solid line correspond to the bubble radial dynamics predicted by the present model. The dashed line is for the model of Lohse and co-workers. Note the logarithmic scale on the vertical axis.

Since the stability equation is linear, the absolute magnitude of the result is immaterial and we have adjusted the scale so as to show the great similarity of the results given by the two methods of calculation. Qualitatively, for small radii, one finds a mild amplification which, for a fairly sharply determined value of the equilibrium radius R_0, increases significantly. It would be possible to designate this value of R_0 as the threshold for the manifestation of this instability. However, without a precise knowledge of the initial amplitude, it is impossible to say whether the resulting amplification will lead to a break-up of the bubble or not.

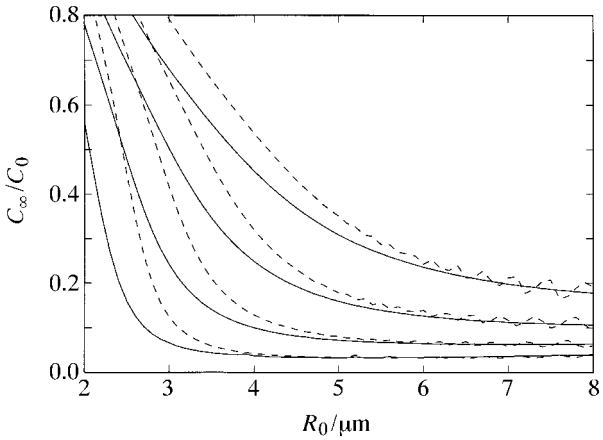

Figure 13. Rectified diffusion thresholds for argon bubbles in water at 26.5 kHz as computed with the present model (solid lines) and the model of Lohse and co-workers (dashed lines). In descending order, the lines correspond to $P_A = 1$, 1.05, 1.1 and 1.15 bar.

Be that as it may, since, as already observed in § 4, the outward acceleration $\ddot{R}$ of the model (2.10), (2.11) is much smaller than that of (2.8), and since the after-bounces are strongly damped in our model, one would expect a far smaller amplification of the surface deformation. The results of the integration of (5.1) with $R(t)$ predicted by the present model for a constant forcing are shown in figure 12, where they are compared with those of Hilgenfeldt *et al.* (1996). Note that we have had to recur to a logarithmic scale to present the two sets of results on the same graph. This finding strongly suggests that the Rayleigh–Taylor instability is not a concern with a thermofluid mechanic model of the bubble interior more precise than that of Lohse *et al.* Hence, we shall not consider this instability further.

6. Mass diffusion

Lohse and co-workers used the following result, due to Fyrillas & Szeri (1994), for the rectified diffusion threshold into a bubble immersed in a liquid with a dissolved gas concentration C_∞ far from the bubble:

$$\frac{C_\infty}{C_0} = \frac{1}{P_\infty + 2\sigma/R_0} \frac{\displaystyle\int_0^{2\pi/\omega} p(t) R^4(t)\,\mathrm{d}t}{\displaystyle\int_0^{2\pi/\omega} R^4(t)\,\mathrm{d}t}, \tag{6.1}$$

where C_0 is the saturation concentration, i.e. the equilibrium gas concentration corresponding to the pressure $P_\infty + 2\sigma/R_0$. The averages over an oscillation cycle indicated on the right-hand side are readily calculated on the basis of the results of the model of §§ 2 and 3. We compare the results of the present model (solid lines) with those of the model of Lohse and co-workers (dashed lines) in figures 13 and 14. The former figure is for $1 \leqslant P_A \leqslant 1.15$ bar, while the latter is for $1.2 \leqslant P_A \leqslant 1.4$ bar. Each pair of lines corresponds to a fixed pressure amplitude.

A qualitatively interesting difference between the two sets of results is the near-absence of oscillations in the present model. The oscillations exhibited by the dashed

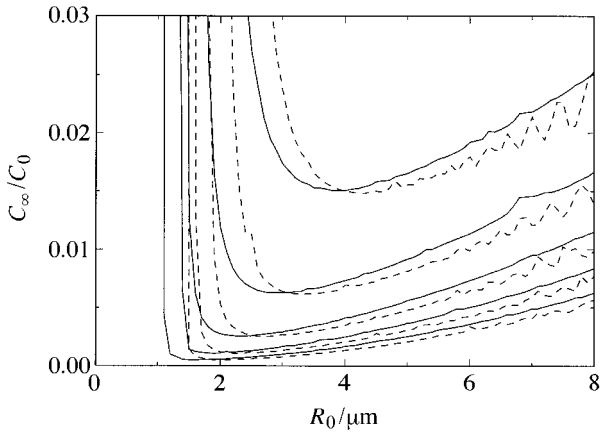

Figure 14. Rectified diffusion thresholds for argon bubbles in water at 26.5 kHz as computed with the present model (solid lines) and the model of Lohse and co-workers (dashed lines). In descending order, the lines correspond to $P_A = 1.2$, 1.25, 1.3, 1.35 and 1.4 bar.

lines are due to a form of resonance of the radial pulsations (Hilgenfeldt *et al*. 1996, 1998) that are suppressed by the more realistic damping of the radial motion embodied in our formulation. Hilgenfeldt *et al*. (1996) discuss the possibility that these oscillations give rise to multiple stable equilibria. It appears that, on the basis of the present calculations, the consequences of this mechanism, if any, are minor.

Other than for this difference, the results of the two models are qualitatively similar. For the stability of the bubble against mass diffusion, the interesting region is that where the slope is positive. For a fixed C_∞/C_0, the present model shifts this region somewhat to the left in the direction of smaller bubble radii.

7. Gas temperature and radial velocity

Two other parameters that arise in the theory of Lohse *et al*. are the radial velocity and the gas temperature. In the theory of these authors the former should exceed the speed of sound in the gas (estimated at the undisturbed temperature) for a shock wave to develop, while the latter should exceed the dissociation temperature of the non-inert gases in the bubble. For nitrogen this temperature is about 9000 K. The corresponding thresholds are shown in figures 15 and 16. In both cases the results given by the present model are lower than those of the model of Lohse and co-workers in the range of pressure amplitudes of interest. To understand this behaviour we show in figure 17 the normalized maximum radius during the steady oscillations as a function of the equilibrium radius for an acoustic pressure amplitude of 1.3 bar. The prominent maxima predicted by both models are due to the well-known rapid disappearance of the inhibiting effect of surface tension with increasing radius (see, for example, Flynn 1964, figure 10). Figure 17 shows that the model of Lohse *et al*. results in a somewhat 'stiffer' bubble, with the result that the oscillation amplitude is larger for the present model.

The maximum of figure 17 is essentially a dynamical analogue of the well-known

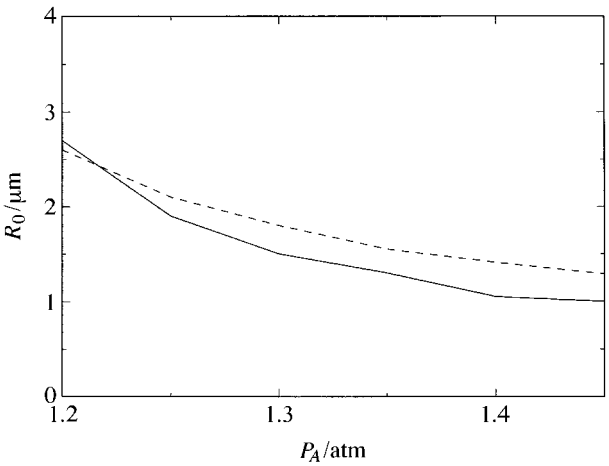

Figure 15. Threshold for the bubble-wall velocity to exceed the speed of sound in the undisturbed gas according to the present model (solid line) and the model of Lohse *et al*. (dashed line).

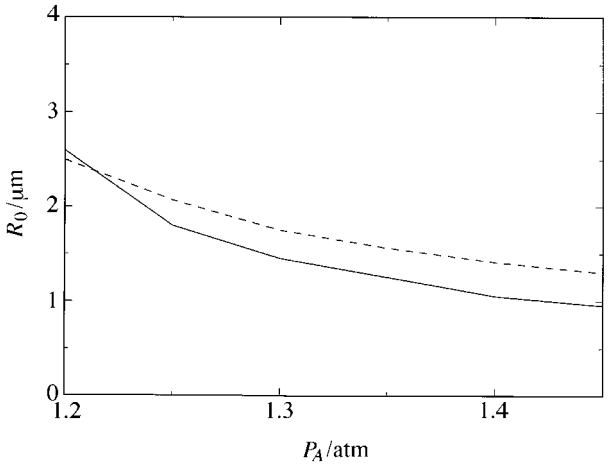

Figure 16. Threshold for the bubble-centre temperature to exceed 9000 K according to the present model (solid line) and the model of Lohse *et al*. (dashed line).

static Blake threshold R_B that, in the present model, would be given by

$$R_B = \frac{4}{3}\frac{\sigma}{|-P_A|}. \tag{7.1}$$

For the case of figure 17, this expression gives $R_B = 0.72\,\mu m$. As shown by Akhatov *et al*. (1997), this 'dynamic Blake threshold' is also essential to explain the minimum in the diffusion threshold curves of figure 14 and, therefore, the diffusional stability of the bubble.

8. The phase diagram

According to the model of Lohse and co-workers, stable sonoluminescence requires that:

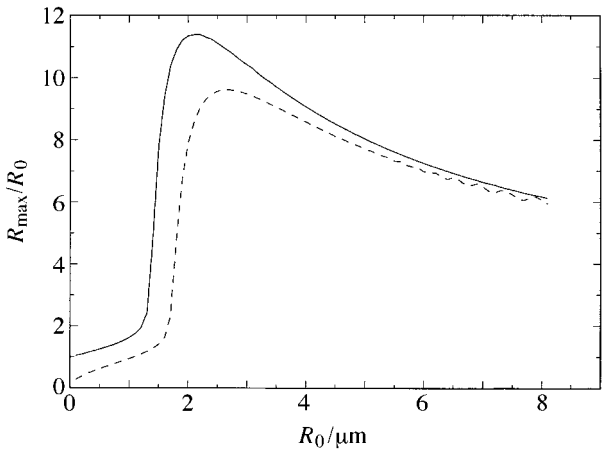

Figure 17. Maximum bubble radius in the course of a steady oscillation normalized by the equilibrium radius as a function of the equilibrium radius according to the present model (solid line) and the model of Lohse *et al*. (dashed line). The acoustic pressure amplitude is 1.3 bar.

(A) the spherical shape be stable;

(B) the bubble be stable against mass diffusion;

(C) the centre temperature exceeds the dissociation temperature of the polyatomic gases in the bubble; and

(D) the bubble-wall Mach number exceeds unity.

It has already been mentioned that more recent work (see, for example, Yuan *et al*. 1998; Vuong *et al*. 1999; Hilgenfeldt *et al*. 1999) has considerably downplayed the importance of shocks, in the first place because shocks may not form in typical conditions, and also because they do not seem necessary to achieve temperatures sufficient to explain the light emission. In any event, one finds that the thresholds for (C) and (D) are very nearly coincident (as can be seen in figures 15 and 16), so that one does not need to consider condition (D) specifically. It is also found in the parameter range we have investigated that condition (B) is more stringent than either (C) or (D). In effect, therefore, the boundaries for sonoluminescent emission are dictated by conditions (A) and (B), the former responsible for the upper boundary, the latter for the lower boundary.

These boundaries are plotted in figure 18, which shows in the concentration–acoustic pressure plane the region for stable sonoluminescence at 26.5 kHz. As before, the solid lines are the present results and the dashed lines those of Lohse and co-workers. The lower boundary is practically unchanged. The upper boundary that we find is shifted upward with respect to the model of Lohse *et al*. by a considerable margin. It would be interesting to investigate experimentally the new region of parameter space suggested by the present calculations.

In figure 19, we compare the boundaries calculated by the present model for a frequency of 26.5 kHz (solid) with those predicted at 15 kHz (short dashes) and at 40 kHz (long dashes). The frequency dependence is quite marked and appears to be a potentially useful and stringent test of the theory.

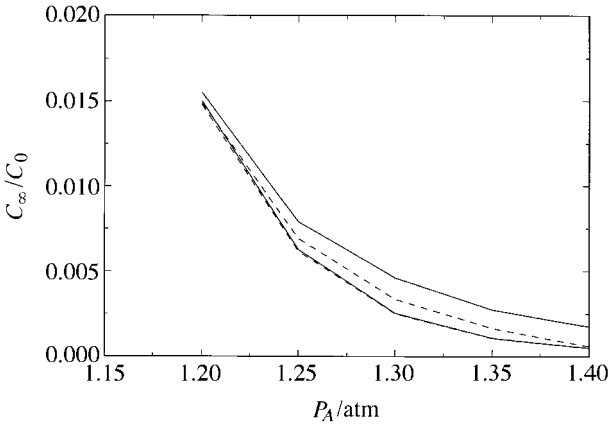

Figure 18. Phase diagram for stable sonoluminescence according to the present model (solid lines) and the model of Lohse *et al*. (dashed lines) at 26.5 kHz.

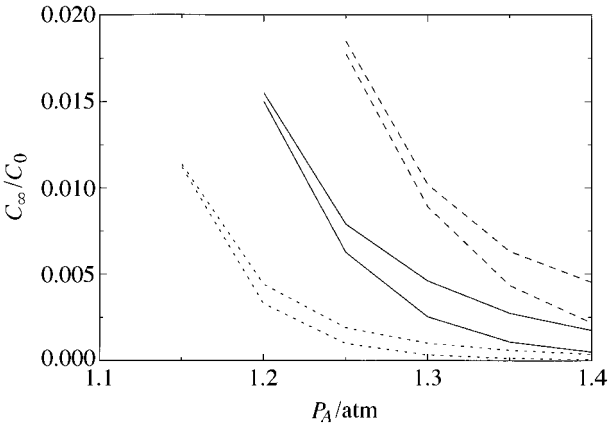

Figure 19. Phase diagram for stable sonoluminescence according to the present model at 15 kHz (short dashes), 26.5 kHz (solid) and 40 kHz (long dashes).

9. Conclusions

In this paper we have examined several features of gas-bubble oscillations on the basis of a mathematical model developed in our earlier papers. It has been found that, even though the bubble-radius-versus-time predicted by various models does not exhibit great differences, several derived quantities are affected more than expected. This conclusion is due to the fact that the radius is obtained by carrying out a repeated integration of the internal pressure, an operation that erases several details of the time dependence of this quantity. Since the thresholds for rectified diffusion and spherical stability depend directly on the pressure and the radial acceleration, they are affected much more than the radius.

Our model for the bubble interior is less sophisticated than others used in the literature (see, for example, Moss *et al*. 1994, 1997; Vuong & Szeri 1996; Vuong *et al*. 1999; Yuan *et al*. 1998), but this has enabled us to present results for steady-state oscillations. This is important as conditions in the bubble interior can differ

considerably between the first cycle and the steady state (see, for example, Kamath *et al*. 1992).

While the conclusions of any numerical calculation must be treated with care due to the modelling aspects that are inherent to any such exercise, this is particularly true in the case of large-amplitude spherical-bubble oscillations. In the first place, sphericity is itself an issue in the presence of acoustic pressure gradients. Secondly, uncertainties exist in the treatment of the liquid compressibility and temperature. Thirdly, the thermofluid mechanics of the bubble interior always seems to probe the mathematical models near their limit of validity or, more likely, beyond. The present results are certainly not immune from these uncertainties and they should be considered more as establishing trends of variation of the various quantities. From this point of view, the frequency dependence shown in figure 19 is particularly interesting. Experiments at different frequencies would be of considerable interest in assessing the importance of the neglected effects and the overall robustness of the model.

The authors thank Professor D. Lohse for clarifications about his methods and Dr R. G. Holt and Dr F. Gaitan for making their shape stability data available. This study has been supported by NASA and the Office of Naval Research.

References

Akhatov, I., Gumerov, N., Ohl, C. D., Parlitz, U. & Lauterborn, L. 1997 The role of surface tension in stable single-bubble sonoluminescence. *Phys. Rev. Lett.* **78**, 227–230.

Amdur, I. & Mason, E. A. 1958 Properties of gases at very high temperatures. *Phys. Fluids* **1**, 370–383.

Apfel, R. E. 1981 Acoustic cavitation. In *Methods of experimental physics* (ed. P. D. Edmonds), vol. 19, pp. 355–411. New York: Academic.

Barber, B. P., Hiller, R. A., Löfstedt, R., Putterman, S. J. & Weninger, K. R. 1997 Defining the unknowns of sonoluminescence. *Phys. Rep.* **281**, 65–143.

Brenner, M. P., Lohse, D. & Dupont, T. F. 1995 Bubble shape oscillations and the onset of sonoluminescence. *Phys. Rev. Lett.* **75**, 954–957.

Brenner, M. P., Lohse, D., Oxtoby, D. & Dupont, T. F. 1996 Mechanism for stable single bubble sonoluminescence. *Phys. Rev. Lett.* **76**, 1158–1161.

Chu, M. C. 1996 The homologous contraction of a sonoluminescing bubble. *Phys. Rev. Lett.* **76**, 4632–4635.

Cole, R. H. 1948 *Underwater explosions*. Princeton University Press (1965 New York: Dover, reprinted).

Flynn, H. G. 1964 Physics of acoustic cavitation in liquids. In *Physical acoustics—principles and methods* (ed. W. P. Mason), vol. 1B, pp. 57–172. New York: Academic.

Fyrillas, M. M. & Szeri, A. J. 1994 Dissolution or growth of soluble spherical oscillating bubbles. *J. Fluid Mech.* **277**, 381–407.

Gaitan, D. F. & Crum, L. A. 1990 Observation of sonoluminescence from a single, stable cavitation bubble in a water/glycerine mixture. In *Frontiers in nonlinear acoustics* (ed. M. Hamilton & D. T. Blackstock), pp. 459–463. New York: Elsevier.

Gaitan, D. F., Crum, L. A., Church, C. C. & Roy, R. A. 1992 Sonoluminescence and bubble dynamics from a single, stable, cavitation bubble. *J. Acoust. Soc. Am.* **91**, 3166–3183.

Hao, Y. & Prosperetti, A. 1999 Viscous effects on the spherical stability of bubbles. *Phys. Fluids*. (In the press.)

Herring, C. 1941 Theory of the pulsations of the gas bubble produced by an underwater explosion. OSRD Rep. no. 236.

Hilgenfeldt, S., Lohse, D. & Brenner, M. P. 1996 Phase diagrams for sonoluminescing bubbles. *Phys. Fluids* **8**, 2808–2826.

Hilgenfeldt, S., Lohse, D. & Moss, W. C. 1998 Water temperature dependence of single bubble sonoluminescence. *Phys. Rev. Lett.* **80**, 1332–1335.

Hilgenfeldt, S., Grossman, S. & Lohse, D. 1999 Sonoluminescence under Occam's razor. *Nature*. (In the press.)

Holt, R. G. & Gaitan, D. F. 1996 Observation of stability boundaries in the parameter space of single bubble sonoluminescence. *Phys. Rev. Lett.* **77**, 3791–3794.

Ilinskii, Yu. A. & Zabolotskaya, E. A. 1992 Cooperative radiation and scattering of acoustic waves by gas bubbles in liquids. *J. Acoust. Soc. Am.* **92**, 2837–2841.

Kamath, V. & Prosperetti, A. 1989 Numerical integration methods in gas-bubble dynamics. *J. Acoust. Soc. Am.* **85**, 1538–1548.

Kamath, V., Oğuz, H. N. & Prosperetti, A. 1992 Bubble oscillations in the nearly adiabatic limit. *J. Acoust. Soc. Am.* **92**, 2016–2023.

Kamath, V., Prosperetti, A. & Egolfopoulos, F. 1993 A theoretical study of sonoluminescence. *J. Acoust. Soc. Am.* **93**, 248–260.

Keller, J. B. & Kolodner, I. I. 1956 Damping of underwater explosion bubble oscillations. *J. Appl. Phys.* **27**, 1152–1161.

Keller, J. B. & Miksis, M. J. 1980 Bubble oscillations of large amplitude. *J. Acoust. Soc. Am.* **68**, 628–633.

Kondić, L., Gersten, J. I. & Yuan, C. 1995 Theoretical studies of sonoluminescence radiation: radiative transfer and parametric dependence. *Phys. Rev.* E **52**, 4976–4990.

Kondić, L., Yuan, C. & Chan, C. K. 1998 Ambient pressure and single bubble sonoluminescence. *Phys. Rev.* E **57**, R32–R35.

Leighton, T. G. 1994 *The acoustic bubble*. London: Academic.

Lepoint, T., De Pauw, D., Lepoint-Mullie, F., Goldman, M. & Goldman, A. 1997 Sonoluminescence: an alternative 'electrohydrodynamic' hypothesis. *J. Acoust. Soc. Am.* **101**, 1–19.

Lezzi, A. & Prosperetti, A. 1987 Bubble dynamics in a compressible fluid. II. Second-order theory. *J. Fluid Mech.* **185**, 289–321.

Löfstedt, R., Barber, B. P. & Putterman, S. J. 1993 Toward a hydrodynamic theory of sonoluminescence. *Phys. Fluids* A **5**, 2911–2928.

Lohse, D. & Hilgenfeldt, S. 1997 Inert gas accumulation in sonoluminescing bubbles. *J. Chem. Phys.* **107**, 6986–6997.

Lohse, D., Brenner, M. P., Dupont, T. F., Hilgenfeldt, S. & Johnston, B. 1997 Sonoluminescing air bubbles rectify argon. *Phys. Rev. Lett.* **78**, 1359–1362.

Longuet-Higgins, M. S. 1996 Shedding of vortex rings by collapsing cavities, with application to single-bubble sonoluminescence. *J. Acoust. Soc. Am.* **100**, 2678.

Longuet-Higgins, M. S. 1997 Particle drift near an oscillating bubble. *Proc. R. Soc. Lond.* A **453**, 1551–1568.

Longuet-Higgins, M. S. 1998 Viscous streaming from an oscillating spherical bubble. *Proc. R. Soc. Lond.* A **454**, 725–742.

Matula, T. J., Cordry, S. M., Roy, R. A. & Crum, L. A. 1997 Bjerknes force and bubble levitation under single-bubble sonoluminescence conditions. *J. Acoust. Soc. Am.* **102**, 1522–1527.

Moss, W. C., Clarke, D. B., White, J. W. & Young, D. A. 1994 Hydrodynamic simulations of bubble collapse and picosecond sonoluminescence. *Phys. Fluids* A **6**, 2979–2985.

Moss, W. C., Clarke, D. B. & Young, D. A. 1997 Calculated pulse widths and the spectra of a single sonoluminescing bubble. *Science* **276**, 1398–1401.

Plesset, M. S. & Prosperetti, A. 1977 Bubble dynamics and cavitation. *Ann. Rev. Fluid Mech.* **9**, 145–185.

Prosperetti, A. 1977*a* Thermal effects and damping mechanisms in the forced radial oscillations of gas bubbles in liquids. *J. Acoust. Soc. Am.* **61**, 17–27.

Prosperetti, A. 1977*b* Viscous effects on perturbed spherical flows. *Q. Appl. Math.* **34**, 339–352.

Prosperetti, A. 1977*c* On the stability of spherically symmetric flows. *Atti Accad. Naz. Lincei, Rend. Cl. Sci. Fis. Mat. Nat.* **62**, 196–203.

Prosperetti, A. 1984*a* Bubble phenomena in sound fields. I. *Ultrasonics* **22**, 69–77.

Prosperetti, A. 1984*b* Bubble phenomena in sound fields. II. *Ultrasonics* **22**, 115–124.

Prosperetti, A. 1991 The thermal behaviour of oscillating gas bubbles. *J. Fluid Mech.* **222**, 587–616.

Prosperetti, A. 1997 A new mechanism for sonoluminescence. *J. Acoust. Soc. Am.* **101**, 2003–2007.

Prosperetti, A. & Lezzi, A. 1986 Bubble dynamics in a compressible liquid. I. First-order theory. *J. Fluid Mech.* **168**, 457–478.

Prosperetti, A., Crum, L. A. & Commander, K. W. 1988 Nonlinear bubble dynamics. *J. Acoust. Soc. Am.* **83**, 502–514.

Trilling, L. 1952 The collapse and rebound of a gas bubble. *J. Appl. Phys.* **23**, 14–17.

Vokurka, K. 1986 Comparison of Rayleigh's, Herring's, and Gilmore's model of gas bubbles. *Acustica* **59**, 214–219.

Vuong, V. Q. & Szeri, A. J. 1996 Sonoluminescence and diffusive transport. *Phys. Fluids* **8**, 2354–2364.

Vuong, V. Q., Szeri, A. J. & Young, D. A. 1999 Shock formation within sonoluminescence bubbles. *Phys. Fluids* **11**, 10–17.

Yuan, L., Cheng, H. Y., Chu, M. C. & Leung, P. T. 1998 Physical parameters affecting sonoluminescence: a self-consistent hydrodynamic study. *Phys. Rev.* E **57**, 4265–4280.

PHILOSOPHICAL TRANSACTIONS OF THE ROYAL SOCIETY A MATHEMATICAL, PHYSICAL & ENGINEERING SCIENCES

PHILOSOPHICAL TRANSACTIONS OF THE ROYAL SOCIETY A MATHEMATICAL, PHYSICAL & ENGINEERING SCIENCES